arXiv:0708.1345v1 [cond-mat.mtrl-sci] 9 Aug 2007

Probing the Electronic Structure of Bilayer Graphene by Raman Scattering

L. M. Malard[1], J. Nilsson[2], D. C. Elias[1], J. C. Brant[1], F. Plentz[1], E. S. Alves[1], A. H. Castro Neto[2] and M. A. Pimenta[1]
[1] *Departamento de Física, Universidade Federal de Minas Gerais, 30123-970, Belo Horizonte, Brazil*
[2] *Department of Physics, Boston University, 590 Commonwealth Avenue, Boston, MA 02215, USA*

(Dated: February 1, 2008)

The electronic structure of bilayer graphene is investigated from a resonant Raman study using different laser excitation energies. The values of the parameters of the Slonczewski-Weiss-McClure model for graphite are measured experimentally and some of them differ significantly from those reported previously for graphite, specially that associated with the difference of the effective mass of electrons and holes. The splitting of the two TO phonon branches in bilayer graphene is also obtained from the experimental data. Our results have implications for bilayer graphene electronic devices.

PACS numbers: 63.20.Kr, 73.21.-b, 78.30.-j, 81.05.Uw

After the development of the phenomenological Slonczewski-Weiss-McClure (SWM) model for the electronic structure of 3D graphite 50 years ago [1, 2], many experimental works were devoted to evaluate the parameters of this standard model [3, 4]. In particular, the weak interaction between two layers in graphite, ascribed to van der Waals forces, can be described by the interlayer SWM parameters, that give, for example, the difference between the effective masses of electrons and holes near the Dirac point (K point in the graphite Brillouin zone) [4]. This work shows that, by performing Raman scattering experiments in bilayer graphene with many different laser excitation energies, we can probe its electronic structure by obtaining experimental values for the SWM parameters. Our values for some interlayer parameters differ significantly from values measured previously for graphite [3, 4], showing that open issues about graphite can now be experimentally revisited using graphene samples [5]. Furthermore, while the unbiased bilayer graphene is a zero-gap semiconductor, a biased bilayer is a tunable gap semiconductor by electric field effect [6, 7]. Hence, the development of bilayer graphene-based bulk devices depends on the detailed understanding of its electronic properties.

Fig. 1 shows the atomic structure of a bilayer graphene, in which we can distinguish the two nonequivalent atoms A and B in each plane giving rise to a unit cell with four atoms. Since this unit cell is the same for graphite in the Bernal stacking structure, we can describe the electronic spectrum of bilayer graphene in terms of the SWM model for graphite [1, 2], by determining the parameters γ_0, γ_1, γ_3 and γ_4, that are associated with overlap and transfer integrals calculated for nearest neighbors atoms. The pair of atoms associated with these parameters are indicated in the atomic structure of a bilayer graphene shown in Fig. 1(a). These parameters, that are fundamental for the electronic processes in the system, are only roughly known to this date.

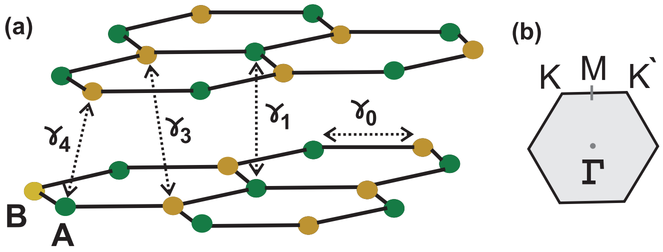

FIG. 1: (a) Atomic structure of bilayer graphene. The A atoms of the two layers are over each other, whereas the B atoms of the two layers are displaced with respect to each other. The SWM constants γ_0, γ_1, γ_3 and γ_4 label the corresponding pair of atoms associated with the hopping processes. (b) First Brillouin zone of monolayer graphene, showing the high symmetry points Γ, K, K′ and M.

The graphene samples used is this experiment were obtained by a micro-mechanical cleavage of graphite on the surface of a Si sample with a 300 nm layer of SiO_2 on the top [5]. The bilayer flakes were identified by the slightly color change from monolayer graphene in an optical microscope, followed by a Raman spectroscopy characterization using the procedure described by Ferrari *et al.* [8]. For the Raman measurements, we used a Dilor XY triple monochromator in the back scattering configuration. The spot size of the laser was $\sim$1 μm using a 100 × objective and the laser power was kept at 1.2 mW in order to avoid sample heating. Raman spectra were obtained for 11 different laser lines of Ar-Kr and dye lasers in the range 1.91–2.71 eV.

Recently, Ferrari *et al.* [8] showed that Raman spectroscopy can be used to identify the number of layers in a graphene sample and, in particular, to clearly distinguish a monolayer from a bilayer graphene sample. Figure 2 shows the Raman spectra of the monolayer [Fig. 2(a)] and bilayer [Fig. 2(b)] graphene samples, where the most prominent features are the G and G′ Raman bands [9]. The G′ band of the monolayer graphene is nicely fitted by just one Lorentzian, whereas four Lorentzian peaks are necessary to fit the G′ band of the bilayer graphene, in agreement with the previous Raman studies of graphene systems [8, 10, 11].

The Raman spectra of both the monolayer and bilayer graphene have been measured with many different laser energies in the visible range. Figure 3 shows the

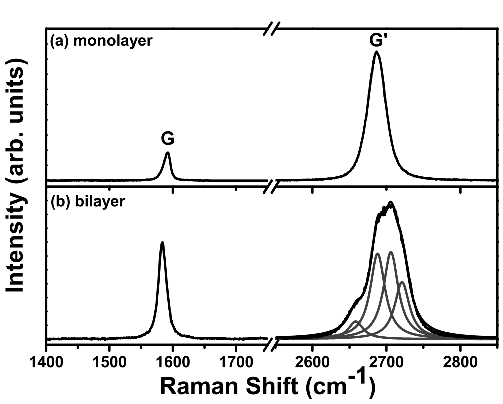

FIG. 2: (a) Raman spectrum of the monolayer graphene and (b) Raman spectrum of the bilayer graphene performed with the 2.41 eV laser line. The G′ band of bilayer graphene is fit with four different Lorentzians with FWHM of ∼ 24 cm^{-1}.

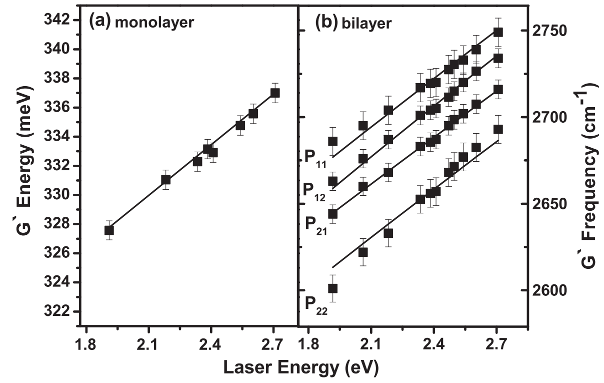

FIG. 3: (a) Laser energy dependence of the G′-band energy for a monolayer graphene. (b) Laser energy dependence of the positions of the four peaks that comprise the G′-band of bilayer graphene. These four Raman peaks originate from the P$_{11}$, P$_{12}$, P$_{21}$ and P$_{22}$ DR processes illustrated in Fig. 4. The black squares are the experimental data and the full lines are the fitted curves (see discussion in the text).

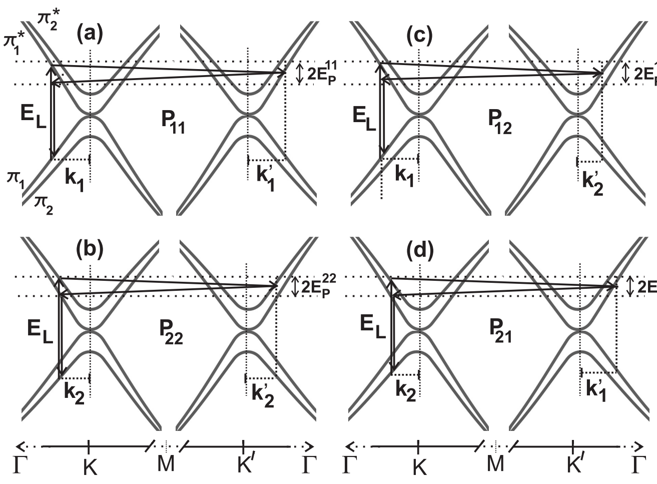

FIG. 4: Schematic view of the electron dispersion of bilayer graphene near the K and K′ points showing both π_1 and π_2 bands. The four DR processes are indicated: (a) process P$_{11}$, (b) process P$_{22}$, (c) process P$_{12}$, and (d) process P$_{21}$. The wavevectors of the electrons (k_1, k_2, k'_1 and k'_2) involved in each of these four DR processes are also indicated.

laser energy dependence of the G′-band frequency for the monolayer sample [Fig. 3(a)] and for each one of the four peaks that comprise the G′ band for bilayer graphene [Fig. 3(b)].

The origin of the G′ band in all graphitic materials is due to an inter-valley double-resonance (DR) Raman process involving electronic states near two nonequivalent K points (K and K′) in the 1st Brillouin zone of graphene [see Fig. 1(b)], and two phonons of the iTO branch [9, 12, 13]. As a result of the angular dependence of the electron-phonon matrix elements [14] and the existence of interference effects in the Raman cross-section [15], the main contribution for the G′-band comes from the particular DR process that occurs along the Γ-K-M-K′-Γ direction, in which the wavevectors k and k' of the two intermediate electronic states in the conduction band (measured from the K and K′ points, respectively) are along the KΓ and K′Γ directions, respectively [8]. Therefore, the wavevector q of the phonons involved in this specific process is along the KM direction and is related to the electron wavevectors by the condition $q = k + k'$ [9].

In the case of the bilayer graphene, where the two graphene layers are stacked in a Bernal configuration [9], the π-electrons dispersion in the valence and in the conduction band splits into two parabolic branches near the K point [16], as shown in Fig. 4. In this figure, the upper and lower branches of the valence band are labeled as π_1 and π_2, respectively. The lower and upper branches of the conduction band are called π_1^* and π_2^*, respectively. Along the high symmetry Γ-K-M-K′-Γ direction, these branches belong to different irreducible representations of the P6$_3$/mmc space group and, therefore, only the $\pi_1 \rightleftarrows \pi_1^*$ and $\pi_2 \rightleftarrows \pi_2^*$ optical transitions between the valence and conduction bands are allowed. Therefore, there are four possible intervalley DR processes involving electrons along the Γ-K-M-K’-Γ direction that lead to the observation of the four peaks of the G′-band of bilayer graphene [8].

The four DR processes are represented in Fig. 4. In process P$_{11}$ [Fig. 4(a)], an electron with wavevector k_1 is resonantly excited from the valence band π_1 to the conduction band π_1^* by absorbing a photon with energy E_L. This electron is then resonantly scattered to a state with wavevector k'_1 by emitting a phonon with momentum q$_{11}$ and energy E_p^{11}. Finally, the electron is scattered back to state k_1 by emitting a second phonon, and it recombines with a hole producing a scattered photon with an energy $E_S = E_L - 2E_p^{11}$. The phonon wavevector q$_{11}$, measured from the K point and along the KM direction, is given by $q_{11} = k_1 + k_1'$.

Fig. 4(b) shows the DR process P_{22}, which involves an electron that is optically excited between the π_2 and π_2^* branches. The energy of the associated phonon is E_p^{22} and its wavevector is given by $q_{22} = k_2 + k_2'$. Figures 4(c) and 4(d) show processes P_{12} and P_{21}, that involve electrons with wavevectors k_1, k_2' and k_2, k_1', respectively, which belong to different electron branches. The wavevectors of the phonons associated with processes P_{12} and P_{21} are given by $q_{12} = k_1 + k_2'$ and $q_{21} = k_2 + k_1'$, respectively.

The two iTO phonon branches of a bilayer graphene along the ΓKM line belong to the irreducible representations T_1 and T_3. The scattering of an electron in the conduction band between states around K and K′ has to satisfy the electron-phonon selection rule, so that the allowed transitions are $\pi_1^* \rightleftarrows \pi_1^*$ or $\pi_2^* \rightleftarrows \pi_2^*$ for the T_1 phonon and $\pi_2^* \rightleftarrows \pi_1^*$ for the T_3 phonon. Since processes P_{11} and P_{22} involves electrons states around K and K′ which belong to the same electronic branch, the associated phonons belong to the T_1 phonon branch. On the other hand, phonons involved in processes P_{12} and P_{21} belong to the T_3 branch.

From Fig. 4 one can see that the phonon associated with the P_{11} process has the largest wavevector (q_{11}). Since the energy of the iTO phonon increases with increasing q, the highest frequency component of the G′-band of a bilayer graphene is related to the P_{11} process. On the other hand, P_{22} process is associated with the smallest phonon wavevector q_{22}, and gives rise to the lowest frequency component of the G′-band of a bilayer graphene. The two intermediate peaks of the G′-band are associated with processes P_{12} and P_{21}.

In order to analyze the experimental results shown in Fig. 3(b), we must find a relation between the electronic and the phonon dispersions of a bilayer graphene, according to the DR Raman process. The electronic dispersion of the bilayer graphene can be described in terms of the standard SWM model for graphite (see e.g. Eq. (2.1) in Ref. [1]) and using the full tight-binding dispersion introduced originally by Wallace [17]. Along the $K - \Gamma$ direction this amounts to replacing σ by $\gamma_0\left[2\cos(2\pi/3 - ka\sqrt{3}/2) + 1\right]$ in McClure's expressions. Here k is measured from the K point and $a = 1.42$ Å is the in plane nearest neighbor carbon distance. Since there is no k_z-dependence we may set $\Gamma = 1$ and $\gamma_2 = \gamma_5 = 0$ (γ_2 and γ_5 correspond to 3^{rd} layer interactions in graphite). We have verified that the parameter Δ does not make any noticeable difference in our results and will be ignored in our analysis. With these simplifications, the bands in the bilayer are parameterized by the four parameters γ_0, γ_1, γ_3 and γ_4. A more detailed account on this approach to the band structure calculation of the graphene bilayer can be found in Ref. [21].

In fact, along the high symmetry $K - \Gamma$ direction, the 4×4 matrix factorizes and the dispersion of the four bands are given by:

$$\begin{aligned} E_{\pi_2} &= (-\gamma_1 - v_3\sigma - \xi_+)/2, && \text{(1a)}\\ E_{\pi_1} &= (\gamma_1 + v_3\sigma - \xi_-)/2, && \text{(1b)}\\ E_{\pi_1^*} &= (-\gamma_1 - v_3\sigma + \xi_+)/2, && \text{(1c)}\\ E_{\pi_2^*} &= (\gamma_1 + v_3\sigma + \xi_-)/2, && \text{(1d)} \end{aligned}$$

where

$$\xi_\pm = \sqrt{(\gamma_1 - v_3\sigma)^2 + 4(1 \pm v_4)^2\sigma^2}, \qquad (2)$$

and $v_j \equiv \gamma_j/\gamma_0$.

In order to obtain the dependence of the phonon energy E_p^{ij} on the laser energy E_L, let us consider a generic process P_{ij}, where i, j = 1 or 2, which describes the four processes shown in Fig. 4. In the first step of this process (electron-hole creation), the incident photon is in resonance with the electronic states in the valence and conduction bands at the k_i point. Thus, the laser energy E_L can be written as:

$$E_L = E_{\pi_i^*}(k_i) - E_{\pi_i}(k_i). \qquad (3)$$

Eq. 3 allows us to determine the momentum k_i of the electron excited in the process.

The electron is then resonantly scattered from the vicinity of the K point to the vicinity of the K′ point by emitting a (iTO) phonon with energy E_p^{ij} given by:

$$E_p^{ij}(k_i + k_j') = E_{\pi_i^*}(k_i) - E_{\pi_j^*}(k_j') \qquad (4)$$

Assuming that we know the iTO phonon dispersion near the K point $[A + B(k_i + k_j')]$ as well as the bands involved (Eqs. 1 and 2), Eq. 4 uniquely determine the momentum of the scattered electron k_j'. We then compute the phonon energy E_p^{ij}, that is directly related to the Raman shift for this specific P_{ij} process, obtained with a given laser energy E_L. Finally, we perform a least-squares fit to determine the parameters γ_0, γ_1, γ_3 and γ_4 of the model (Eqs. 1 and 2) that give the best fit of the dispersion of the four G′ peaks in bilayer graphene shown in Fig. 3. The four solid lines in Fig. 3(b) represent the best fitting of the experimental E_p^{ij} versus E_L data.

We have also tried to fit, unsuccessfully, our experimental data for the four DR processes taking only γ_0, γ_1 and γ_3. Therefore, in order to get a good fitting, the parameter γ_4 value, that is associated with the splitting of the two G′ intermediate peaks, has to be included. For the dispersion of the iTO phonon branches near the K point, we could not fit satisfactorily the dispersion data in Fig. 3(b) considering the same phonon dispersion for the four P_{ij} processes. The best fit was obtained when we considered different dispersions for the two iTO phonon branches of bilayer graphene. Table I shows the parameters obtained for each phonon branch, which exhibit a linear dispersion near the K point. Notice that the difference between these two phonon branches corresponds to a splitting of about 3 cm^{-1}, which is in close agreement to that reported previously [8, 11].

TABLE I: Values obtained for the phonon dispersion of the two iTO phonon branches of bilayer graphene near the K point, where E_p^{ii}=A$_{ii}$+B$_{ii}$q corresponds to the P$_{11}$ and P$_{22}$ processes and E_p^{ij}=A$_{ij}$+B$_{ij}$q to the P$_{12}$ and P$_{21}$ processes.

A_{ii}	B_{ii}	A_{ij}	B_{ij}
153.7 (meV) 1238 (cm^{-1})	38.5 (meV Å) 310 (cm^{-1} Å)	154.0 (meV) 1241 (cm^{-1})	38.8 (meV Å) 313 (cm^{-1} Å)

Table II shows the γ values obtained experimentally. The parameter γ_0, associated with the in-plane nearest-neighbor hopping energy, is ten times larger than γ_1, which is associated with atoms from different layers along the vertical direction (see Fig. 1). These values are in good agreement with the previous angle resolved photoemission spectroscopy (ARPES) measurements in bilayer graphene [22]. The resolution of our experiment allows, however, the measurement of weaker hopping parameters (γ_3 and γ_4) , that are beyond the current resolution of ARPES. The value of γ_1 is about three times larger than γ_3 and γ_4, both associated with the interlayer hopping not along the vertical direction (see Fig. 1).

The corresponding parameters found experimentally for graphite are also shown in Table II [3, 4]. The parameters γ_0 and γ_1 for bilayer graphene are slightly smaller than those for graphite. This difference is more accentuated for the parameter γ_3. Notice that our value for γ_3 is in good agreement with that reported theoretically by Tatar and Rabii [18]. On the other hand, our value of γ_4 for bilayer graphene is significantly higher than the value for graphite measured by Mendez *et al.* in a magnetoreflection experiment. [19]. Moreover, this parameter is specially important since it is related to the difference of electron and hole effective masses in the valence and conduction bands [4]. This is particularly important in the context of the biased bilayer graphene [6]. We must stress that our value for γ_4 is in good agreement with the calculations performed by Tatar and Rabii [18] and by Charlier *et al.* [20].

TABLE II: Experimental SWM parameters (in eV) for the band structure of bilayer graphene. The parameters for graphite are taken from Refs. 3, 4.

	γ_0	γ_1	γ_2	γ_3	γ_4	γ_5	$\gamma_6 = \Delta$
Bilayer graphene	2.9	0.30	n/a	0.10	0.12	n/a	n/a
Graphite	3.16	0.39	-0.02	0.315	0.044	0.038	0.008

In summary, from the resonant Raman study of the G′-band of bilayer graphene using several laser excitation energies, we have been able to probe the dispersion of electrons and phonons of this material near the Dirac point. From the fitting of the experimental data using the SWM model, we have obtained experimental values for hopping parameters for bilayer graphene. The parameters γ_3 and γ_4 found here differ significantly from the values previously measured for graphite [3, 4, 19], showing that open issues about graphite can now be revisited using graphene samples. The slight difference between the experimental and theoretical data in Fig. 3(b), specially for lower laser energies, might be ascribed to many-body effects in bilayer graphene [23]. Finally, in a future work we will study DR processes involving holes as well as the biased bilayer graphene.

This work was supported by Rede Nacional de Pesquisa em Nanotubos de Carbono - MCT, Brasil and FAPEMIG. L.M.M., J.C.B and D.C.E. acknowledge the support from the Brazilian Agency CNPq. We would like to thank Millie Dresselhaus and Ado Jorio for critical reading of the manuscript and for helpful discussions.

[1] J. W. McClure, Phys. Rev. **108**, 612 (1957).

[2] J. C. Slonczewski and P. R. Weiss, Phys. Rev. **109**, 272 (1958).

[3] N. B. Brandt and S. M. Chudinov and Ya. G. Ponomarev, *Semimetals 1: Graphite and its Compounds*, North-Holland (Amsterdam) 1988.

[4] M.S. Dresselhaus, G. Dresselhaus, K. Sugihara, I. L. Spain and H. A. Goldberg, *Carbon Fibers and Filaments, Chapter 7*, Springer Verlag (Berlin Heidelberg) 1988.

[5] A. K. Geim and K. S. Novoselov, Nature Materials **6**, 183 (2007).

[6] E. V. Castro *et al.*, cond-mat/0611342.

[7] J. B. Oostinga *et al.*, cond-mat/0707.2487.

[8] A. C. Ferrari *et al.*, Phys. Rev. Lett. **97**, 187401 (2006).

[9] M. A. Pimenta *et al*, Phys. Chem. Chem. Phys. **9**, 1276 (2007).

[10] A. Gupta *et al.*, Nano Lett. **6**, 2667 (2006).

[11] D. Graf *et al.*, Nano Lett. **7**, 238 (2007).

[12] C. Thomsen and S. Reich, Phys. Rev. Lett. **85**, 5214 (2000).

[13] R. Saito *et al.*, Phys. Rev. Lett. **88**, 027401 (2002).

[14] G. Ge. Samsonidze. Photophysics of Carbon Nanotubes. PhD thesis, Department of Electrical Engineering and Computer Science, Massachusetts Institute of Technology, February 2007.

[15] J. Maultzsch *et al.*, Phys. Rev. B **70**, 155403 (2004).

[16] E. McCann and V. I. Falko, Phys. Rev. Lett. **96**, 086805 (2006).

[17] P. R. Wallace, Phys. Rev. **71**, 622 (1947).

[18] R. C. Tatar and S. Rabii, Phys. Rev. B **25**, 4126 (1982).

[19] E. Mendez, A. Misu and M. S. Dresselhaus, Phys. Rev. B **21**, 827 (1980).

[20] J.-C. Charlier *et al.*, Phys. Rev. B **46**, 4531 (1992).

[21] B. Partoens and F. M. Peeters, Phys. Rev. B. **74**, 075404 (2006).

[22] T. Ohta *et al.*, Phys. Rev. Lett. **98**, 206802 (2007).

[23] S. Viola Kusminskiy *et al.*, cond-mat/0706.2359.